Report of
Project "*Understanding of catalysis on early transition metal oxide-based catalysts through exploration of surface structure and chemistry during catalysis using in-situ approaches*"

Report from previous grant period

A report of progress of research project funded by the catalysis science program of BES of DOE (Grant No. DE-SC0008625 entitled "*Understanding of catalysis on early transition metal oxide-based catalysts through exploration of surface structure and chemistry*") is presented here by first summarizing the motivation and objectives of the current project and then describing the research activity we have performed and the scientific insights and achievement we have obtained so far.

1. Summary of motivation and objectives of the project (*Understanding of catalysis on early transition metal oxide-based catalysts through exploration of surface structure and chemistry during catalysis using in-situ approaches)*

Two main categories of heterogeneous catalysts are metal and metal oxide which catalyze 80% chemical reactions at solid-gas and solid-liquid interfaces. Metal oxide catalysts are much more complicated than metal catalysts. The reason is that the cations of the metal atoms could exhibit a few different oxidation states on surface of the same catalyst particle such as Co_3O_4 or change of their oxidation states under different reactive environments. For a metal catalyst, there is only one oxidation state typically. In addition, surface of a metal oxide can be terminated with multiple surface functionalities including O atoms with different binding configurations and OH group. For metal, only metal atoms are exposed typically. Obviously, the complication of surface chemistry and structure of a metal oxide makes studies of surface of an oxide catalyst very challenging. Due to the complication of surface of a meal oxide, the electronic and geometric structures of surface of a metal oxide and the exposed species have received enormous attention since oxide catalysts catalyze at least 1/3 chemical reactions in chemical and energy industries.

Understanding of catalytic reactions on early transition metal oxide-based catalysts is fundamentally intriguing and of great practical interest in energy- and environment-related catalysis. Exploration of surface chemistry of oxide-based catalysts at molecular level during catalysis has remained challenging though it is critical in deeply understanding catalysis on oxide-based catalysts and developing oxide-based catalysts with high activity and selectivity. Thus, the overall objective of this project is to explore surface chemistry and structure of early transition metal oxide-based catalysts through in-situ characterization of surface of catalysts, measurements of catalytic performances, and then build an intrinsic correlation of surface chemistry and structure with their catalytic performances in a few important catalytic reactions, and essentially fundamentally understand catalytic mechanism. Furthermore, this correlation will guide the design of catalysts with high activity and selectivity.

2. Brief of research achievements of the project funded by DOE

With the supported of the current DOE project we have mainly studied Co_3O_4-based, CeO_2-based, and RhO-based catalysts. We mainly used a lab-based ambient pressure X-ray photoelectron spectrometer using monochromated Al Kα (AP-XPS) and high pressure scanning tunneling microscopy (HP-STM) to track surface chemistry (oxidation state, surface composition, electronic state) and surface structure (atomic arrangement, binding configurations of adsorbate, surface phase transformation) under reaction condition and during catalysis. Here "under reaction condition" is defined to a characterization of a catalyst in a gaseous environment of one reactive gas such as H_2 or O_2; "during catalysis" is defined to a characterization of a catalyst in gaseous environment of all reactant gases.

In the last 2-3 years of this project (September 2012-Nov 2015) funded by the catalysis science program of BES of DOE, we have performed the following work: (1) a lab-based Al Kα AP-XPS was installed; (2) a high pressure STM was built[1]; (3) in-situ studies of surface chemistry of Co_3O_4 and Co_3O_4-based catalyst during water gas-shift and design of a new bi-functional catalyst, Pt-Co alloy nanoclusters supported on nonstoichiometric CoO_{1-x} bimetallic catalysts[2]; (4) preparation and in-situ studies of Co-Ru bimetallic layers on Co_3O_4 nanorods for reduction of CO_2[3]; (5) catalysis and in-situ studies of CeO_2 with doped metal cations for generation of syngas through partial oxidation of CH_4[4]; (6) catalysis and in-situ studies of reduction of NO with CO on nonstoichiometric CoO_{1-x}[5-7]; (7) catalysis and in-situ studies of water-gas shift on mesoporous CeO_2 loaded with metal nanoclusters consisting curvy metal-oxide interface[8]; (8) chemical transformation of methane to methanol[9] and acetic acid[10] through oxidation in solutions, (9) in-situ studies of surface oxide, Rh(110)-1×2-O at atomic scale during CO oxidation[11,12]. Through financial support from the catalysis program of BES of DOE, about 15 papers were accepted [1-8,12-18] and five manuscript were submitted[7,9-11,19] and five will be submitted[20-24]. PI delivered about 8 invited talks/lectures of these results achieved through financial support from DOE-BES catalysis science program.

In terms of the Co_3O_4-based catalyst series, we prepared Co_3O_4 nanorods with preferentially exposed (110) surface. Our catalytic measurement shows it is active for water-gas shift[2]. In-situ studies suggest that surface oxygen valences could be active for dissociating H_2O and cobalt cations for adsorbing CO. By anchoring Pt-Co nanoclusters (1-2 nm) on Co_3O_4, a highly active WGS catalyst was prepared. In-situ photoemission features from AP-XPS studies show that the substrate oxide is in fact CoO formed through a phase transformation from Co_3O_4.[2] This catalyst consists of CoO and Pt-Co bimetallic nanoclusters. It exhibit an activation barrier of only 24.8 kJ/mol. In addition, in-situ observation using AP-XPS revealed a phase transformation from Co_3O_4 to CoO in the reactant gas (CO+NO) in the temperature range of 200-300ºC[5]; the newly formed CoO is nonstoichiometric and highly active for reduction of NO with CO in the temperature range of 225-600ºC with a high thermal stability. Surface oxygen vacancies are suggested to be the site for dissociation of NO; Co^{2+} is the sites to adsorb CO molecule.

For CeO_2-based catalysis, mesorporous CeO_2 was prepared. A following deposition of metal precursors to mesoporous channels formed Pd, Pt, Cu, Au nanoclusters. In these catalysts, M@mp-CeO_2, the metal-oxide interface is unique[8]. It is a curvy interface instead of an open, flat interface of metal nanoparticles supported on CeO_2 cubic parties. This bent interface results in a high catalytic activity evidenced by the low activation barrier of WGS and high TOF. In addition, through integrating metal cations to CeO_2 lattice of bulk, Pd, Pt, and Rh cations were successfully doped to CeO_2. It is active for methane partial oxidation to generate syngas. The three catalyst exhibit quite different catalytic performances. This differences were well rationalized with in-situ surface chemistry identified with AP-XPS. CeO_2 doped with Rh cations exhibits highest activity and thermal stability up to 600ºC. The lack of phase separation of Rh cations results from the strong binding of Rh-O bonds.

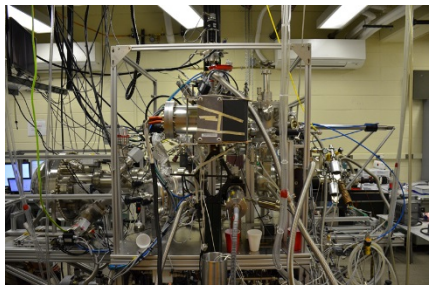

Figure 1. *Photo of lab-based Al Kα AP-XPS daily available in PI group for in-situ studies.*

3. Research activities performed so far funded by the catalysis program of DOE-BES

3.1 Development of ambient pressure XPS (AP-XPS) and ambient pressure high temperature STM (AP-HT-STM)

Since 2013, PI's group has built a new ambient pressure XPS (AP-XPS) by using monochromated Al Kα and Energy analyzer (Figure 1) through a collaboration with one manufacturer in European country and a partial support with external funds. In addition, a high pressure scanning tunneling microscope (Figure

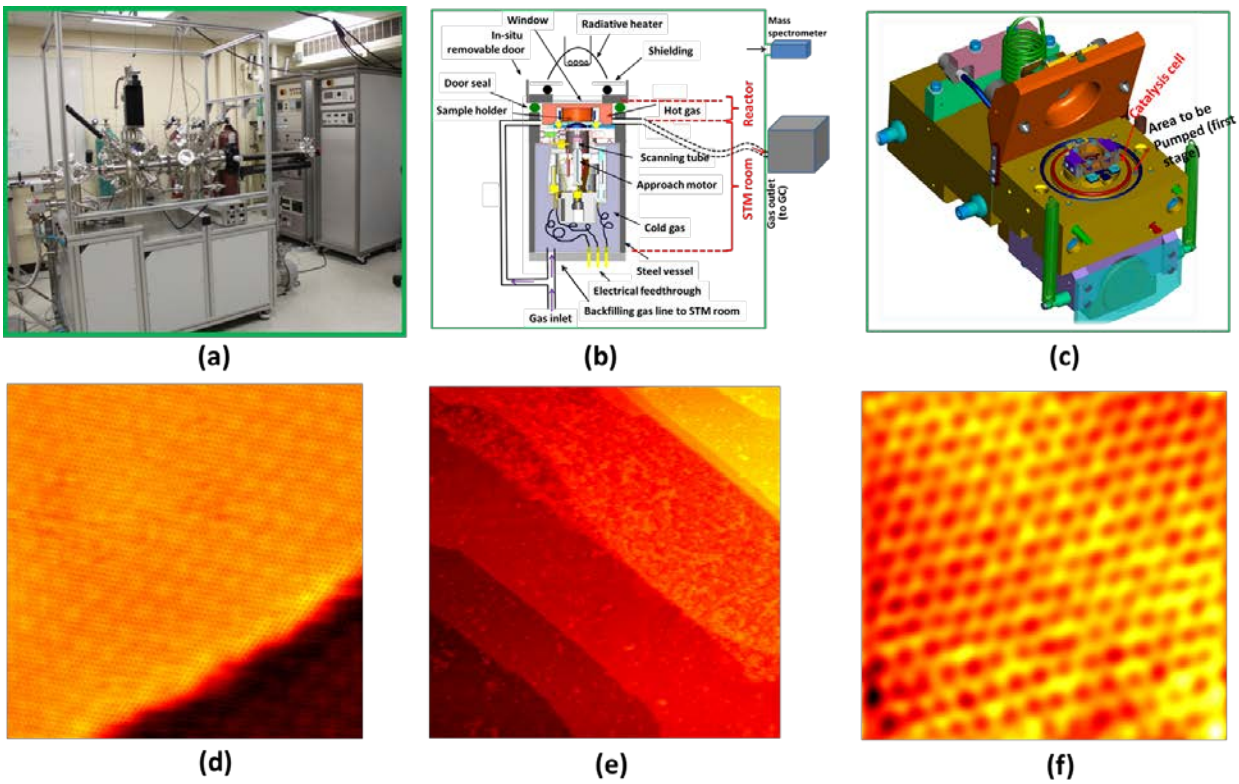

Figure 2. *High pressure STM in PI group. (a) Photo of the whole system. (b) Integration catalytic reaction cell to STM room. (c) Assembly of reaction cell to STM room. (d) Atom-resolved Pt(111) in 1 Torr CO. (e) and (f) Atom-resolved graphene in 25 Torr N_2 at 230°C.*

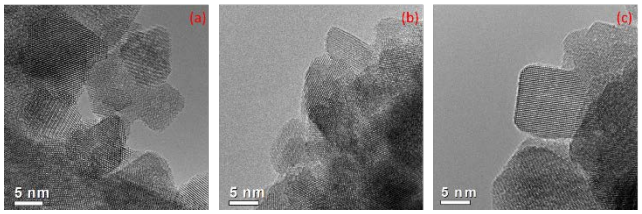

Figure 3. *TEM images of Pd-CeO_2-air (a), Pt-CeO_2-air (b), and Rh-CeO_2-air (c).*

2) was designed through support from startup of university. The two instruments are the routine characterization tools of PI group. [1]

For the purpose of in-situ studies of catalyst surface under reaction condition or during catalysis, a reaction cell was installed. In our lab-based AP-XPS, the reaction cell is a flowing cell (Figure 1b). Flow rate is about 4 ml/min without opening the valve of gas exit. By gradually opening the valve on gas exit line, flow rate can be increased to 10-15 ml/min. For each reactant, we typically use a tank of pure gas as its gas source. Thus, 4 ml/min in the reaction cell is equal to 80 ml/min 5% reactant gas (balanced with Ar or He) used in fixed-bed flow reactor. Thus, the flow rate of the reaction cell of AP-XPS is similar to that of a fixed-bed flow reactor. By having such a flowing reaction cell, the diffusion limitation of product molecules is avoid; otherwise, the re-adsorption of product molecules could give unpredictable influence on surface chemistry and structure of the catalyst. The much smaller volume of the reaction cell (about 20-50 ml of empty volume) compared to a UHV chamber, typically 10-20 liters offers the capability of readily heating up to 650°C when the sample is in a gas with a pressure 25 Torr, or 750°C when the sample is in a gas with a pressure 5 Torr. R4000 Hipp-3 energy analyzer was used for this purpose. As shown in Figure 3, Au 4f spectra of Au foil in 20 Torr of N_2 with quite reasonable signal/noise ratio were achieved.

Another technique we used for this project is the high pressure STM. A reaction cell (Figure 2b) was designed. The reaction cell was integrated with the STM room consisting of a coarse approaching motor and scanning tube and STM tip (Figure 2b). The purpose to have this flowing cell is to allow a gas to flow through a hot catalyst during STM characterization. As shown in Figure 2b, the tip can penetrate an aperture with a diameter of <0.5 mm and access to surface of the catalyst which is at certain temperature

and in gas phase with certain pressure. The HP-STM allows us for visualizing surface of a catalyst at high temperature in a gas phase with certain pressure. The functions of the aperture is to allow tip to access the catalyst surface and to minimize thermal diffusion of hot gas to the catalyst. A flow rate of 4 ml/min can be achieved. It is comparable to the flow rate of AP-XPS. Thus, a model catalyst such as Rh(110)-2×1-O can be studied with AP-XPS and HP-STM in parallel under the exact same experimental conditions. As shown in Figures 2d and 2e, atomic resolved images of Pt(111) in CO at RT and graphene on Rh(0001) at 230°C were achieved.

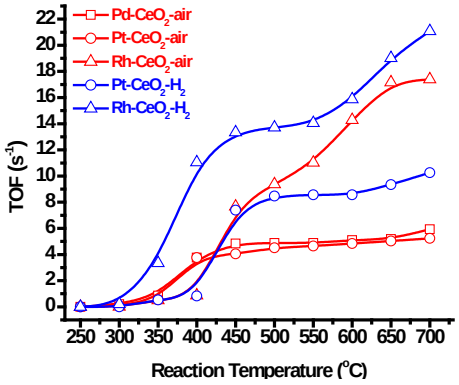

Figure 5. *TOF of Pd-CeO_2-air, Pt-CeO_2-air, and Rh-CeO_2-air at different temperature.*

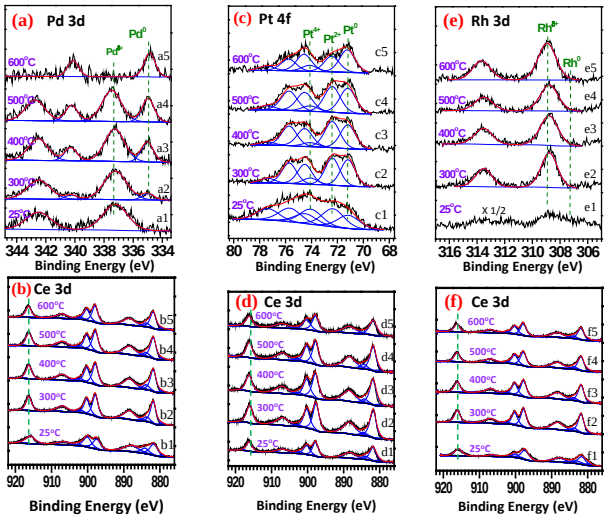

Figure 4. *In-situ AP-XPS studies of catalyst during methane partial oxidation. (a) Pd 3d of Pd-CeO_2-air. (b) Ce 3d of Pd-CeO_2-air. (c) Pt4f of Pt-CeO_2-air. (d) Ce 3d of Pt-CeO_2-air. (e) Rh 3d of Rh-CeO_2-air. (f) Ce 3dof Rh-CeO_2-air.*

3.2 In-situ studies of CeO_2 with doped Pd, Pt, and Rh for methane partial oxidation to form syn gas

Methane partial oxidation (MPO) chemically transforming natural gas into syngas for the production of gasoline is one of the reaction channels to utilize CH_4 since synas can be used for the production of gasoline or methane through Fischer-Tropsch synthesis. Three catalysts, CeO_2 with doped Pd, Pt, and Rh were synthesized. To prepare the doped catalyst, precursors of Pd, Pt, and Rh were mixed with precursor of Ce ations. A hypothermal synthesis with a following calcination offers these catalysts. As shown in Figure 3, Pd, Pt, and Rh were doped in the lattice of CeO_2.[4] No additional phase of metal or metal oxide except CeO_2 was identified with XRD. The cationic state of these doped Pd, Pt, and Rh was further confirmed with their photoemission features of the as-synthesized catalysts (Figures 4a, 4c, and 4e). These catalysts are highly active for MPO (Figure 5). Table 1 list the conversion of methane and selectivity for producing CO and H_2 on Pd-CeO_2-air, Pt-CeO_2-air, and Rh-CeO_2-air. Obviously, Rh-CeO_2-air exhibits much better catalytic selectivity. In addition, it also exhibits much higher TOF as seen in Figure 5.

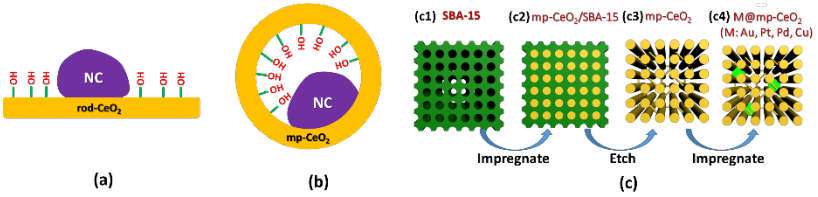

Figure 6*. Structural models of metal nanoclusters supported on CeO_2. (a) Metal NC on flat CeO_2 nanorod. (b) Metal NC encapsulated in a pore of mp-CeO_2. (c) Schematic showing the preparation of mp-CeO_2 with a supported metal NCs on the internal wall of mp-CeO_2.*

Table 1. Catalytic performance of methane partial oxidation on Pd/CeO_2-air, Pt/CeO_2-air, and Rh/CeO_2-air.

Temperature (°C)	Catalyst	X_{CH_4} (%)	S_{H_2} (%)	S_{CO} (%)	H_2:CO ratio
400	Pd/CeO_2-air	28.7	48.4	11.8	7.2
	Pt/CeO_2-air	28.8	44.8	5.8	14.7
	Rh/CeO_2-air	37.4	52.8	11.2	10.4
500	Pd/CeO_2-air	45.9	78.8	43.0	3.7
	Pt/CeO_2-air	43.9	72.2	36.6	4.2
	Rh/CeO_2-air	61.4	83.3	53.3	3.1
600	Pd/CeO_2-air	61.5	87.6	71.2	2.6
	Pt/CeO_2-air	53.1	74.2	56.6	2.6
	Rh/CeO_2-air	83.6	89.9	77.5	2.3
700	Pd/CeO_2-air	84.0	92.5	91.9	2.2
	Pt/CeO_2-air	74.6	88.5	85.8	2.3
	Rh/CeO_2-air	95.2	92.9	85.7	2.2

terms of Rh-CeO_2-air, AP-XPS studies show that Rh-CeO_2-air catalyst remains its cationic state during catalysis in the whole temperature range of RT and 600°C; thus obviously Rh cations and oxygen vacancies are active sites for methane partial oxidation. The different evolution of surface chemistry of the three catalysts (Figure 4) suggest the significance of in-situ studies in understanding catalytic performance and reaction mechanism. The obvious difference in evolution of the oxidation state of Pt, Pd and Rh can be rationalized with the difference in bond strength of M-O and the reducibility of M cations (M=Pd, Pt, or Rh). The strong bond strength of Rh-O and low reducibility of Rh cations were confirmed by the invariation of catalytic performance even if the catalyst was pretreated in H_2 at 600°C (Figure 4e5). The catalytic performance of Rh-CeO_2-air at 600°C does not show any change within 24 hours.[4]

3.3 Shape-dependent catalytic performance of water-gas shift at two different metal/oxide interfaces

Catalysts of metal nanoparticles supported on CeO_2 are active for water-gas shift. In general, it is considered as a bi-functional catalyst although the detailed mechanism is not completely clear. Typically, metal atoms of a metal nanoparticle act as sites for adsorbing CO molecules and oxygen vacancies of reducible oxide for dissociating H_2O molecules. Figure 6a is the schematic of this bi-functional catalyst of metal supported on a reducible oxide.

In situ characterization using AP-XPS shows Pd cations in Pd-CeO_2-air was partially reduced to metallic Pd and eventually completely reduced to Pd nanoparticles at 600°C (Figure 4a5). Although the reactant O_2 and CH_4 are oxidizing and neutral gases, respectively, products CO and H_2 generated during catalysis can reduce the catalysts. At 600°C, the active phase is in fact metallic Pd nanoparticles supported on CeO_2. Pt cations of Pt-CeO_2-air are partially reduced to metallic Pt in all the temperature range (RT-600°C). In

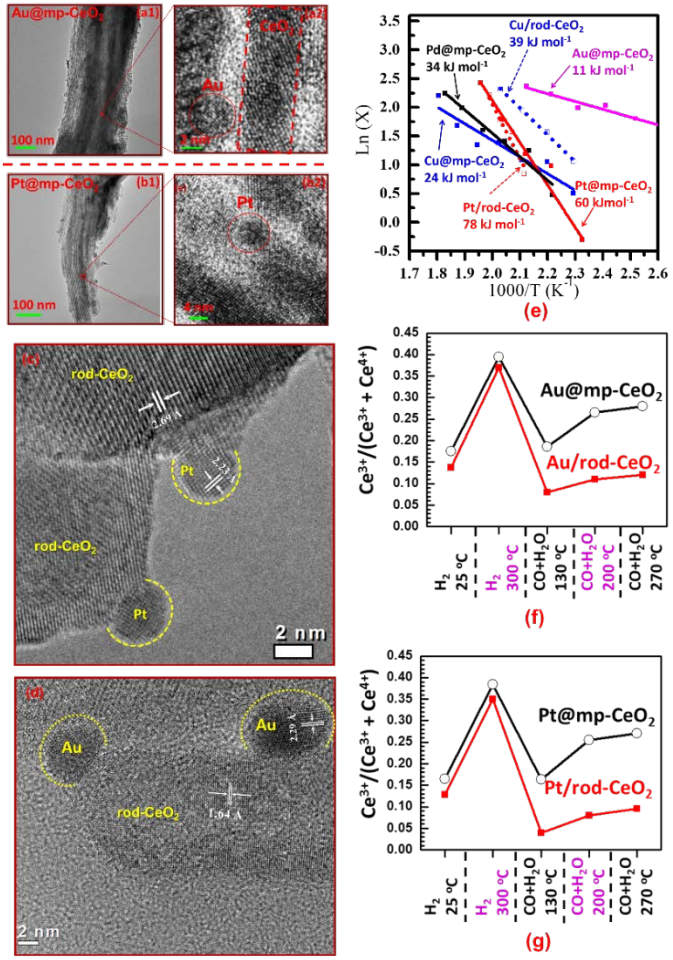

Figure 7. *Catalyst structure and catalytic performance of metal NCs anchored on the internal surface of walls of mp-CeO_2 (M NC@mp-CeO_2) and metal NCs supported on external flat surface of CeO_2 nanocubes. (a) TEM images of Au@mp-CeO_2. (b) TEM images of Pd@mp-CeO_2. (c) TEM image of Pt NCs/rod-CeO_2. (d) TEM image of Au NCs/rod-CeO_2. (e) Arrhenius plots of catalysts. (f) Evolution of oxygen vacancies (presented with atomic ratio Ce^{3+}/Ce^{4+}) of Au@mp-CeO_2 and Au/rod-CeO_2 as a function of reaction conditions. (g) Evolution of oxygen vacancies (presented with atomic ratio Ce^{3+}/Ce^{4+}) of Pt@mp-CeO_2 and Pt/rod-CeO_2 as a function of reaction conditions.*

[4]Mesoporous oxide has been a support for many catalysts since it exhibits high surface area and a reasonable pore size to anchored metal nanoparticles. We synthesized mp-CeO_2 by using mp-SiO_2 as a hard template. After synthesis of mp-silica, precursor of Ce^{3+} was introduced to the pore of mp-SiO_2 (SBA-15); a following calcination will make mp-SiO_2 filled with CeO_2. A dissolution of SiO_2 in NaOH removes the SiO_2 template and thus form mesoporous CeO_2. By deposition precipitation with a following calcination in O_2 and then H_2, metal nanoparticles were introduced and anchored on the infernal surface of wall of mp-CeO_2. Figure 6c is the protocol we used to prepare mp- CeO_2. With this protocol, Au NCs@mp-CeO_2, Pt NCs@mp-CeO_2, Pd NCs@mp-CeO_2, and Cu NCs@mp-CeO_2 were prepared. Figures 7a and 7b present some presentative TEM images of these catalysts. To explore any potential difference in catalytic performance of bent surface of CeO_2 and flat surface, Au NCs supported on CeO_2 (Figures 7c), Pt NCs supported on CeO_2 rods (Figure 7d), Pd NCs supported on CeO_2 rods, and Cu NCs supported on CeO_2 rods were prepared. Catalytic activity (TOF) and activation barriers of the eight catalyst in kinetics control regime were measured under the same condition. Figure 7e presents the activation barrier of these catalysts. They

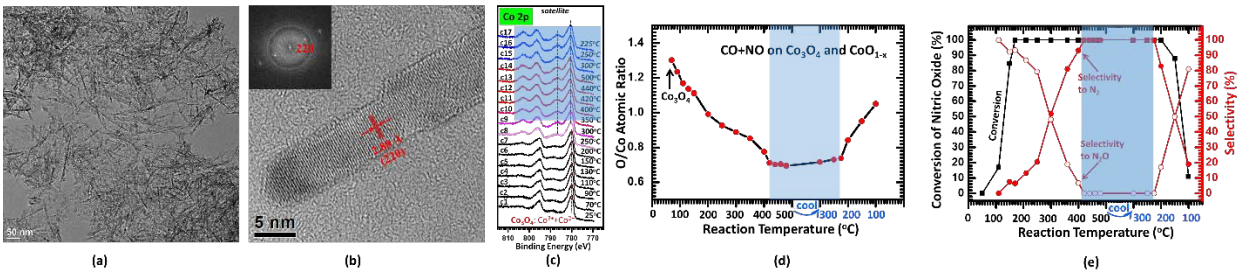

Figure 8. *Preparation, in-situ surface chemistry and catalytic performance of Co_3O_4 nanorods toward identification of the active phase, $CoO_{0.75}$ formed during catalysis. (a and b) TEM images of Co_3O_4 nanorods. (c) Co 2p XPS peaks of Co_3O_4 nanorods at different temperature in the mixture of NO and CO; the light blue region marks the formation of cobalt monoxide surface phase. (d) Quantitative analysis of O/Co atomic ratio as a function of reaction temperature on the mixture of CO and NO; in the temperature region of 425°C-225°C cobalt monoxide is nonstoichiometric. (e) Catalytic performance for reducing NO with CO at different temperature. A correlation between in-situ surface chemistry and catalytic performance shows that non-stoichiometric $CoO_{0.75}$ exhibits a high activity and 100% selectivity for reduction NO with CO to N_2.*

clearly demonstrated a trend that the activation barriers of the M@mp-CeO_2 are lower than those of M/rod CeO_2. These low activation barriers were correlated to the surface chemistry of catalysts during catalysis. We performed in-situ studies of these catalysts during WGS catalysis by using AP-XPS. Oxygen vacancy densities of these samples were examined. As shown in Figure 7f, the internal surface of the walls of Au/mp-CeO_2 has a high density of oxygen vacancies by 10% compared to that of metal NPs on CeO_2 nanorods. The high concentrations of oxygen vacancies on the internal wall of M NCs@mp-CeO_2 (Figures 7f and 7g) during WGS catalysis suggest a low binding energy of OH group on the internal concave wall of mp-CeO_2 during catalysis; the low adsorption energy of OH on the concave surface could contribute to the lower activation energy of WGS on M@mp-CeO_2 compared to M/rod-CeO_2.

3.4 High activity and selectivity of CoO nanorods for reduction of NO with CO

Search of a replacement of precious metal components of catalysts currently for reduction of NO with CO for removal of NO released from exhaust of engine of vehicle is significant since the abundance of Rh used in current three-way catalysts in earth is extremely low. A replacement of such non-renewable source is critical for remaining a sustainable environment. Motivated by this mission, we explored some possible replacement such as cobalt oxides for the reaction of NO reduction with CO. This was inspired by high activity of Co_3O_4 for CO oxidation even at a temperature as low as -80°C[25].

Co_3O_4 nanorods (Figures 8a and 8b) were synthesized with the method reported in literature. The high activity of surface lattice oxygen atoms makes it an active catalyst for reduction of NO with CO.[5] Interestingly, our in-situ studies of Co_3O_4 in the mixture of NO and CO with AP-XPS show that Co_3O_4 is in fact restructured to CoO (Figure 8c)[5]. The appearance of a satellite peak at 768.4 eV is the characteristic peak position of Co 2p of Co^{2+} in CoO. There is no such a peak observed for Co_3O_4. Thus, clearly a phase transformation from Co_3O_4 to CoO is performed. Catalytic measurements of the formed CoO shows high

activity and selectivity. In fact, it exhibits 100% selectivity of NO reduction with CO on CoO in the temperature range of 225°C-600°C. Further quantitative analysis shows that the O/Co ratio of CoO is about 70%-80%. By correlating the surface chemistry (Figures 8c and 8d) and the corresponding catalytic performance (activity and selectivity) for reducing NO with CO (Figure 8e), we assigned the active phase to the nonstoichiometric CoO_{1-x}. Stability test shows no variation of catalytic activity and selectivity for production of N_2 at 420°C within 42 hours.

3.5 Conversion of methane to methanol on a bent mono(μ-oxo)dinickel anchored on internal surface of micro-pores

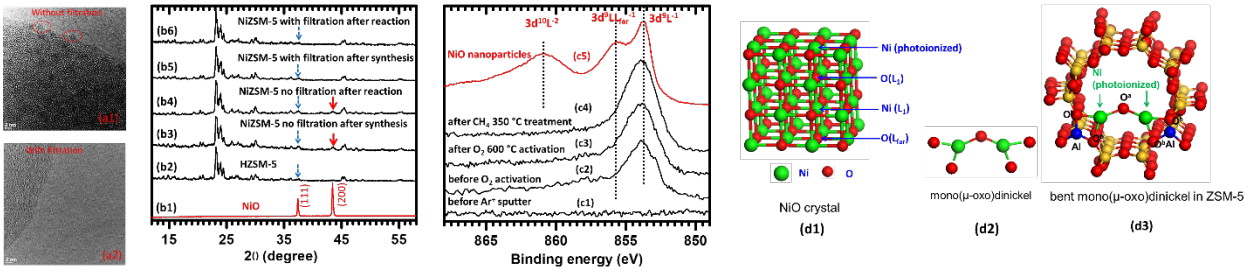

Figure 9. *Characterizations of Ni cations encapsulated in ZSM-5. (a1) TEM image of sample without a filtration step. (a2) TEM image of sample with a filtration step. (b) XRD patterns of samples pretreated with different protocols. (c) XPS studies of Ni 2p photoemission feature of Ni cations of different samples. (d) Strucutrla model of NiO nanoparticles and bent mono(μ-oxo)dinickel in ZSM-5.*

CH_3OH is one of the most important raw materials in chemical industry for production of numerous commodities. In addition, it is an energy carrier to provide energy for portable devices through low-temperature fuel cell technology. Interest in utilization of methanol has largely increased in the recent decade due to the potential for commercialization of low-temperature methanol fuel cell technology. Currently, production of CH_3OH from CH_4 in chemical industries is a two-step process. The first step is conversion of methane to synthesis gas (CO and H_2) by steam reforming of methane[26]; the second step is the synthesis of methanol from CO and H_2[26-29]. Unfortunately, the first step is performed at a rather high temperature of 600-800°C,[26] which significantly increases the energy consumption and the cost of industrial footprint. To economically utilize CH_4 to produce CH_3OH, a process to *directly* synthesize CH_3OH from CH_4 at a *mild condition* is needed. This one-step process is called direct, partial oxidation of methane to methanol. Here it is simply called a direct oxidation of methane to methanol.

From a thermodynamic point of view, synthesis of CH_3OH directly from CH_4 is energetically favorable even at room temperature at ambient pressure of CH_4. However, it is known that activation of the C-H bond of CH_4 is the most challenging elemental step due to the strong C-H bond (436 kJ/mol)[26]. In addition, controllably partial oxidation of CH_4 to a specific fuel molecule, methanol is another challenge since a complete oxidation of CH_4 to CO_2 and H_2O readily happens[30,31] in contrast to partial oxidation. Thus, prevention of a complete oxidation of CH_4 remains quite challenging in the partial oxidation of methane to methanol. In this project, we synthesized Ni-ZSM5 catalysts consisting of bent mono(μ-oxo)dinickel species on the internal wall of ZSM5 by wetness incipience of Ni-precursor and a following activation in O_2. Catalytic measurements show that this Ni-ZSM5 is active for conversion of CH_4 to CH_3OH. In-situ characterizations using multiple techniques show that the active site is bent mono(μ-oxo)dinickel anchored in the ZSM5. To synthesis mono(μ-oxo)dinickel @ZSM5 without any formed nickel oxide nanoclusters, an extra step called filtration is necessary. This step washed out extra nickel cations on external surface of a ZSM5 nanoparticle, only leaving nickel cations on the internal surface of the pores of ZSM5. A precise control of the amount of Ni cations is also important since an extra amount of Ni precursors could form nickel oxide to block the pore.

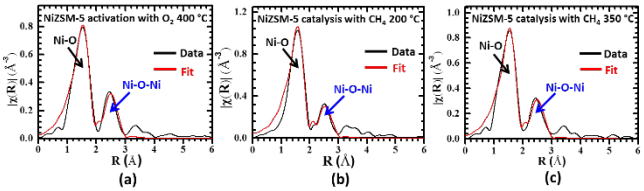

Sample	Binding Environment	$CN_{(O-Ni)}$	$N_{(Ni-O-Ni)}$	R(Å)	σ^2(Å^2)	ΔE_0 (eV)
CH_4 200°C	Ni-Ni′	0				
	O-Ni′	3.0±0.3		2.04±0.01	0.006±0.001	-3.2±0.8
	Ni-O-Ni′		2.0±1.1	2.99±0.02	0.016±0.006	-3.2±0.8
CH_4 350°C	Ni-Ni′	0				
	O-Ni′	2.5±0.3		2.00±0.01	0.006±0.001	-3.2±0.8
	Ni-O-Ni′		2.2±1.1	2.95±0.02	0.016±0.005	-3.2±0.8

Figure 10*. EXAFS studies of catalyst Ni@ZSM-5 under different reaction conditions. (a) Ni-ZSM5 activated with O_2 at 400oC. (b) Ni@ZSM-5 catalysis with CH_4 at 200°C. (c) Ni@ZSM-5 catalysis with CH_4 at 350°C.*

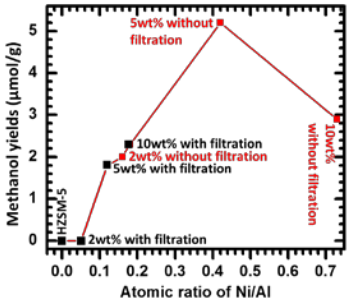

Figure 11. *Yield of methanol from methane partial oxidation on Ni@ZSM5 as a function of atomic ratio of Ni to Al.*

The lack of NiO nanoclustes on the external surface of ZSM5 nanoparticles and internal surface of the pores was confirmed by TEM images and XRD, and XPS respectively[13]. As seen in Figure 10b, there is no any NiO nanoclusters if a filtration step is included; XRD shows the lack of NiO diffraction pattern upon filtration (Figure 10b5); The lack of NiO nanoclusters but existence of Ni cation was confirmed by XPS studies of Ni 2p (Figure 10c2-c4). For NiO nanoclusters (Figure 10c5), the photoionized Ni atom can be neutralized by transferring an electron from one of the oxygen atoms of the second nearest Ni atoms, Ni*-O(L_1)-Ni(L_2)-***O(L_{far})***-Ni(L_4)-O(L_5). The photoionized Ni atom is Ni*; the ligand providing an electron is ***O(L_{far})***[32]; this charge transfer results in a different final state labeled as $3d^9LL_{far}^{-1}$, which corresponds to the strong satellite peak at 856.0 eV (Figure 10c5). Upon sputtering out certain layer of silica, Ni 2p of Ni species in the pores of ZSM5 can be seen (Figures 10c2-c4). Surprisingly, the Ni 2p does not show any satellite peaks other than the main peak of Ni $2p_{3/2}$. Based on the origin of the satellite peak, the lack of this satellite peak shows the lack of Ni-O-Ni-O structure. This deduction was supported by the EXAFS analysis of this catalyst before and after catalysis. Clearly, there is no any distinct binding between Ni and Ni atoms. The low coordination number CN_{O-Ni} is in the range of 2.5±0.5 and 3.0±0.3. It suggests that no NiO nanoclusters were formed on the micro-pores since that coordination number is equal to 6 in NiO nanoparticles. In addition, the coordination of Ni atoms to the Ni atoms in the second shell, 2.0±1.1 suggests the formation of a Ni-O-Ni structure. It also excludes the possibility that -Ni-O-O-Ni- is the main oxide species since Ni atom is found in the second closest shell. Figure 10d3 presents the structural model based on the EXAFS and XPS studies. As shown in Figure 12 this catalyst is active for chemical transformation of methane to methanol in partial oxidation at 175°C.[13]

3.6 Catalytic oxidation of methane to methanol under a mild condition at 150°C on Pd_1O_4@ZSM5 in liquid

There are two limits in the partial oxidation performed on Ni@ZSM-5 in gas phase of CH_4. The strong binding energy of methanol molecules on the internal surface of ZSM-5 makes desorption of the production molecules CH_3OH desorb almost impossibly at reaction temperature of 175°C. A desorption at a temperature of 350°C is possible but oxidation at this temperature will in fact produce CO_2 and H_2O. Thus, typically a dissolution of methanol adsorbed in ZMS-5 with H_2O is the method to separate CH_3OH from ZSM-5. Another disadvantage is the re-generation of active sites. This activation has to be done at 400°C or higher. Strictly speaking, the formation of methanol on Ni@ZMS-5 is not a catalytic process since the a bent mono(μ-oxo)dinickel is consumed after the formation of methanol. Facing this disadvantage, we have prepared Pd_1O_4@ZSM-5 and Rh_1O_5@ZSM-5 which can activate CH_4 under different catalytic conditions at a solid-liquid interface.

Table 2. *TOFs for methane partial oxidation for production on 0.01wt%Pd/ZSM5 and other catalysts which convert CH4 to CH3OH and other organic oxygenates at solid liquid interface.*

Entry	Catalyst	Temp. (°C)	TOF[a] for all organic products	TOF[b] for methanol only	Source
1	0.01wt%Pd/ZSM5	50	2.45	0.16	This work
2	0.01wt%Pd/ZSM5	70	9.70	0.33	This work
3	0.01wt%Pd/ZSM5	95	16.58	0.26	This work
4	0.01wt%Pd/ZSM5+2wt%CuO	50	1.91	1.53	This work
5	0.01wt%Pd/ZSM5+2wt%CuO	70	3.89	3.42	This work
6	0.01wt%Pd/ZSM5+2wt%CuO	95	3.39	2.96	This work
7	2.5wt%Fe/ZSM5	50	0.01	0.001	Ref 1
8	Cu/ZSM5[c] (in gas phase)	200	4.25×10^{-5}	1.17×10^{-5}	Ref 2
9	Au-Pd/TiO_2	90	0.0369	0.0073	Ref 3

[a] $TOF = \frac{moles\ of\ all\ organic\ prodcuts}{moles\ of\ met al \times time\ (in\ second)}$. [b] $TOF = \frac{moles\ of\ met hanol}{moles\ of\ metal \times time\ (in\ second)}$.

[c] *Conversion of CH_4 was performed while Cu/ZSM was in gas phase of CH_4.*

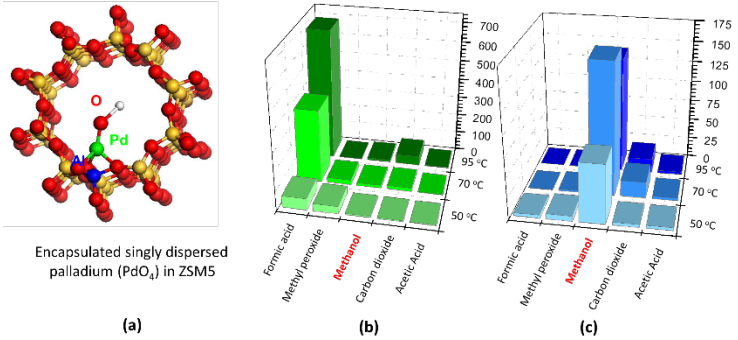

Figure 12. *Strucutral model and catalytic perfomrac of 0.01wt%Pd/ZSM-5. (a) Structural model. (b) Catalytic performance of 0.01wt%Pd/ZSM5 at 50°C, 70°C, and 95°C. (c) Catalytic performacne of 0.01wt%Pd/ZSM with 2wt%CuO at 50°C, 70°C, and 95°C. The amount of catalyst is 28 mg. Pressure of CH_4 is 30 bar. Oxidizing agent is 5 mmol H_2O_2 diluted in 10 ml H_2O. Reaction time is alway 30 minutes upon the correspoing temeprature is reached.*

The singly dispersed Pd_1O_4 species anchored on ZSM-5, Pd_1O_4@ZMS-5 were prepared through three steps: formation of HZSM-5, incipient wetness impregnation of Pd precursor to pores, and drying in vacuum oven with a following calcination for ion exchange. Methane partial oxidation was performed in a high-pressure batch reactor. H_2O_2 mixed in H_2O was used as a liquid oxidizing agent. Catalyst powder was added to the liquid. CH_4 was introduced and kept at a constant pressure in the range of 3-30 bars during catalysis. The solution with a catalyst was heated to certain temperature while it was stirred. EXAFS studies suggest the formation of Pd_1O_4 single site. Catalytic measurement of the Pd_1O_4@ZMS-5 at solid-liquid interface shows that single site Pd_1O_4 is highly active for chemical transformation of methanol by using H_2O_2 as oxidation agent at 50-95°C (Figures 13b and 13c). Table 2 lists the catalytic performance of this catalyst. By depositing CuO nanoparticles on the external surface of Pd_1O_4@ZMS-5, selectivity for production of methanol was largely increased to 90% (Figure 13c) although the overall conversion is decreased. This is because CuO can oxidize H_2O_2 preferentially compared to the oxidation of methanol to formic acid.

References

(1) Tao, F.; Luan, N.; Zhang, S. Design of a new reactor-like high temperature near ambient pressure scanning tunneling microscope for catalysis studies. *Review of Scientific Instruments* **2013**, *84*.

(2) Zhang, S.; Shan, J.-j.; Zhu, Y.; Frenkel, A. I.; Patlolla, A.; Huang, W.; Yoon, S. J.; Wang, L.; Yoshida, H.; Takeda, S.; Tao, F. WGS Catalysis and In Situ Studies of CoO1-x, PtCon/Co3O4, and PtmCom '/CoO1-x Nanorod Catalysts. *Journal of the American Chemical Society* **2013**, *135*, 8283-8293.

(3) Zhu, Y.; Zhang, S.; Ye, Y.; Zhang, X.; Wang, L.; Zhu, W.; Cheng, F.; Tao, F. Catalytic Conversion of Carbon Dioxide to Methane on Ruthenium-Cobalt Bimetallic Nanocatalysts and Correlation between Surface Chemistry of Catalysts under Reaction Conditions and Catalytic Performances. *Acs Catalysis* **2012**, *2*, 2403-2408.

(4) Zhu, Y.; Zhang, S.; Shan, J.-j.; Nguyen, L.; Zhan, S.; Gu, X.; Tao, F. In Situ Surface Chemistries and Catalytic Performances of Ceria Doped with Palladium, Platinum, and Rhodium in Methane Partial Oxidation for the Production of Syngas. *Acs Catalysis* **2013**, *3*, 2627-2639.

(5) Zhang, S.; Shan, J.; Zhu, Y.; Nguyen, L.; Huang, W.; Yoshida, H.; Takeda, S.; Tao, F. Restructuring Transition Metal Oxide Nanorods for 100% Selectivity in Reduction of Nitric Oxide with Carbon Monoxide. *Nano Letters* **2013**, *13*, 3310-3314.

(6) Wang, L.; Zhang, S.; Zhu, Y.; Patlolla, A.; Shan, J.; Yoshida, H.; Takeda, S.; Frenkel, A. I.; Tao, F. Catalysis and In Situ Studies of Rh-1/Co3O4 Nanorods in Reduction of NO with H-2. *Acs Catalysis* **2013**, *3*, 1011-1019.

(7) Shiran Zhang, L. N., Jingxia Liang, Junjun Shan, Jingyue (Jimmy) Liu, Anatoly I. Frenkel, Anitha Patlolla, Jun Li, Franklin (Feng) Tao. Catalysis on Rh-Co sites supported on nonstiochiometric CoO. *Nature Communications* **2014**, *NCOMMS-14-07702A*

(8) Wen, C.; Zhu, Y.; Ye, Y.; Zhang, S.; Cheng, F.; Liu, Y.; Wang, P.; Tao, F. Water-Gas Shift Reaction on Metal Nanoclusters Encapsulated in Mesoporous Ceria Studied with Ambient-Pressure X-ray Photoelectron Spectroscopy. *Acs Nano* **2012**, *6*, 9305-9313.

(9) Nguyen, L. Z., S.; Huang, W.; Li, Y.; Shan, J.; Zeng, S.; Frenkel, A. I.; Tao, F. Catalytic conversion of methane to methanol and formic acid on singly dispersed palladium oxide species on internal surface of ZSM-5. *Chemical Sciences* **2014**, *submitted.*

(10) Nguyen, L. Z., S.; Huang, W.; Li, Y.; Shan, J.; Zeng, S.; Frenkel, A. I.; Tao, F. Transformation of Methane to Acetic Acid through Coupling of Methane, CO, and O2 under a Mild Condition. *Journal of the American Chemical Society* **2015**, *submitted.*

(11) Nguyen, L. L., Lacheng, Tao, Franklin (Feng). In-situ studies of Rh(110) surface under reaction condition with CO and

during CO oxidation *Journal of the American Chemical Society* **2014**, *submitted.*

(12) Zeng, S.; Luan, N.; Cheng, F.; Liu, L.; Yu, Y.; Tao, F. Surface structure and chemistry of Pt/Cu/Pt(111) near surface alloy model catalyst in CO. *Applied Surface Science* **2014**, *320*, 225-230.

(13) Shan, J.; Huang, W.; Luan, N.; Yu, Y.; Zhang, S.; Li, Y.; Frenkel, A. I.; Tao, F. Conversion of Methane to Methanol with a Bent Mono(mu-oxo)dinickel Anchored on the Internal Surfaces of Micropores. *Langmuir* **2014**, *30*, 8558-8569.

(14) Tao, F.; Zhang, S.; Luan, N.; Zhang, X. Action of bimetallic nanocatalysts under reaction conditions and during catalysis: evolution of chemistry from high vacuum conditions to reaction conditions. *Chemical Society Reviews* **2012**, *41*, 7980-7993.

(15) Gu, J.; Zhang, Y.-W.; Tao, F. Shape control of bimetallic nanocatalysts through well-designed colloidal chemistry approaches. *Chemical Society Reviews* **2012**, *41*, 8050-8065.

(16) Pei, Y.; Zhou, G.; Nguyen, L.; Zong, B.; Qiao, M.; Tao, F. Synthesis and catalysis of chemically reduced metal-metalloid amorphous alloys. *Chemical Society Reviews* **2012**, *41*, 8140-8162.

(17) Zhang, S. R. N., L.; Liang, J.; Shan, J.; Liu, J.; Frenkel, A.; Patlolla, A.; Li, J.; Tao, F. Catalysis on sub-nanometer metal particles on oxide support. *Nature Communications* **2015**, *NCOMMS-14-07702A*.

(18) Zhang, S.; Luan, N.; Zhu, Y.; Zhan, S.; Tsung, C.-K.; Tao, F. In-Situ Studies of Nanocatalysis. *Accounts of Chemical Research* **2013**, *46*, 1731-1739.

(19) Jun-jun Shan, L. N., Shiran Zhang,; Ziyuan Wang, L. Z., Zili Wu, Shibi Zeng, Peijun Hu, Franklin (Feng) Tao. Understanding complete oxidation of methane on spinel oxide at molecular level through in-situ studies. *Nature Communications* **2014**, *NCOMMS-14-05692B*.

(20) Nguyen, L. Z., S.; Zhang, S. R.; Tao, F. Preferential Oxidation of CO in H2 on Pure Co3O4. *ACS Catalysis* **2015**, *to be submitted.*

(21) Nguyen, L. Z., S. R.; Frenkel, A. I.; Tao, F. Formation of second generation nanoparticles on surface of metal nanoparticles in reactant gases. *Journal of the American Chemical Society* **2015**, *To be submitted*.

(22) Zhang, S. S., Junjun; Nguyen, Luan; Tao, Franklin (Feng). Complete Combustion Oxidation of Methane on Nonstoichiometric NiO1-x at a Relatively Low Temperature. *Journal of the American Chemical Society* **2015**, *to be submitted.*

(23) Luan Nguyen, S. Z., Junjun Shan, Franklin (Feng) Tao. Evolution of surface chemistry of Co3O4 under various pretreatment conditions for CO oxidation. *Journal of Physical Chemistry C* **2015**, *to be submitted.*

(24) Jun-jun Shan, S. Z., Luan Nguyen, Franklin (Feng) Tao. Mechanistic Understanding of Complete Oxidation of Methane on Fe3O4 Doped with Ni2+through In-situ Studies and Isotope Labelling. *ACS Catalysis* **2015**, *to be submitted.*

(25) Xie, X.; Li, Y.; Liu, Z.-Q.; Haruta, M.; Shen, W. Low-temperature oxidation of CO catalysed by Co3O4 nanorods. *Nature* **2009**, *458*, 746-749.

(26) Ertl, G. K., H.; Schüth, F.; Weitkamp, J.: *Handbook of Heterogeneous Catalysis*; Wiley-VCH, 2008.

(27) Behrens, M.; Studt, F.; Kasatkin, I.; Kuhl, S.; Havecker, M.; Abild-Pedersen, F.; Zander, S.; Girgsdies, F.; Kurr, P.; Kniep, B. L.; Tovar, M.; Fischer, R. W.; Norskov, J. K.; Schlogl, R. The Active Site of Methanol Synthesis over Cu/ZnO/Al2O3 Industrial Catalysts. *Science* **2012**, *336*, 893-897.

(28) Hueso, J. L.; Martinez-Martinez, D.; Caballero, A.; Gonzalez-Elipe, A. R.; Mun, B. S.; Salmeron, M. Near-ambient X-ray photoemission spectroscopy and kinetic approach to the mechanism of carbon monoxide oxidation over lanthanum substituted cobaltites. *Catalysis Communications* **2009**, *10*, 1898-1902.

(29) Vandentop, G. J.; Kawasaki, M.; Nix, R. M.; Brown, I. G.; Salmeron, M.; Somorjai, G. A. FORMATION OF HYDROGENATED AMORPHOUS-CARBON FILMS OF CONTROLLED HARDNESS FROM A METHANE PLASMA. *Physical Review B* **1990**, *41*, 3200-3210.

(30) Coperet, C. C-H Bond Activation and Organometallic Intermediates on Isolated Metal Centers on Oxide Surfaces. *Chemical Reviews* **2010**, *110*, 656-680.

(31) Ding, X. L.; Wu, X. N.; Zhao, Y. X.; He, S. G. C-H Bond Activation by Oxygen-Centered Radicals over Atomic Clusters. *Accounts of Chemical Research* **2012**, *45*, 382-390.

(32) Grosvenor, A. P.; Biesinger, M. C.; Smart, R. S.; McIntyre, N. S. New interpretations of XPS spectra of nickel metal and oxides. *Surface Science* **2006**, *600*, 1771-1779.